One-step synthesis of photoluminescent nanofluids by direct loading of reactively sputtered cubic ZrN nanoparticles into organic liquids

Mariia Protsak,[a] Kateryna Biliak,[a] Daniil Nikitin,[a] Pavel Pleskunov,[a] Marco Tosca,[a,b] Suren Ali-Ogly,[a] Jan Hanuš,[a] Lenka Hanyková,[a] Veronika Červenková,[a] Anastasiya Sergievskaya,[c] Stephanos Konstantinidis,[c] David Cornil,[d] Jérôme Cornil,[d] Miroslav Cieslar,[e] Tereza Košutová,[f] Tomáš Popelář,[g] Lukáš Ondič,[g] Andrei Choukourov[a]*

Electronic Supplementary Information

Details of the conductive AFM measurements

The AFM measurements were performed in ambient air with a relative humidity of 40 % and at room temperature. We used the same highly durable and highly conductive single diamond tip (TipsNano, DEP01, boron-doped diamond, macroscopic resistivity is 0.003-0.005 Ohm×m, tip radius is 7 nm) for all measurements, including scanning in the amplitude modulation intermittent contact mode and acquiring current-voltage (I-V) curves in the contact mode. The spring constant of 1.6 N/m was calculated from the resonant frequency of the cantilever (52 kHz) and its geometrical dimensions using the Sader method. The dependence of the contact force on setpoint was calibrated by acquiring curves of the cantilever deflection versus distance in the contact mode using 100-nm Au-covered silicon as a substrate. All I-V curves were acquired at the same contact force of 20 nN between the tip and the substrate.

For the measurements, we prepared a sub-monolayer of ZrN NPs on Au-covered silicon. The Au film was grounded, while the bias was supplied to the AFM tip. First, the sample was scanned in an intermittent contact mode at scan sizes of 1 × 1 μm and 250 × 250 nm to identify the area of interest (Figure S 1a and b). The device was then switched to a contact mode, the tip was brought into contact with the uncovered Au substrate, and the I-V curves were recorded by applying a voltage bias of -1.0 V – +1.0 V between the tip and the Au film. Then, the instrument feedback was turned off, the tip was positioned on top of a specific ZrN NP, the instrument feedback was turned on, and the I-V curves were recorded. It should be noted that positioning of the tip on top of the ZrN NPs was not always precise because of thermal drifts. On certain occasions, the approaching tip shifted the NPs from their original positions and got in contact with Au instead of ZrN. Obtaining the I-V curve of a shape similar to that of Au was taken as

a criterion of bad positioning, and such data were discarded. Obtaining the I-V curve of a shape significantly different from that of Au was taken as a criterion of good contact. After the I-V measurements, the area of interest was scanned again in the intermittent contact mode to ensure that the topography of the surface and the tip shape did not change (Figure S 1c). Note that one NP (designated by a cross) was moved away from the original position after interaction with the tip, and its I-V curves were discarded.

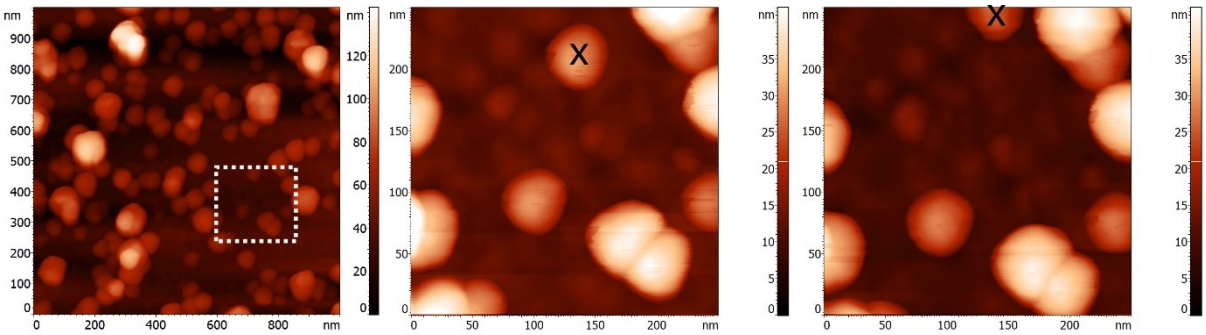

Figure S 1 AFM semicontact height images of ZrN NPs on Au: a) scan size of 1×1 μm before acquiring I-V curves; b) scan size of 250 × 250 nm before acquiring I-V curves; c) scan size of 250 × 250 nm after acquiring I-V curves.

Size distribution of Zr and ZrN NPs calculated from the SEM images

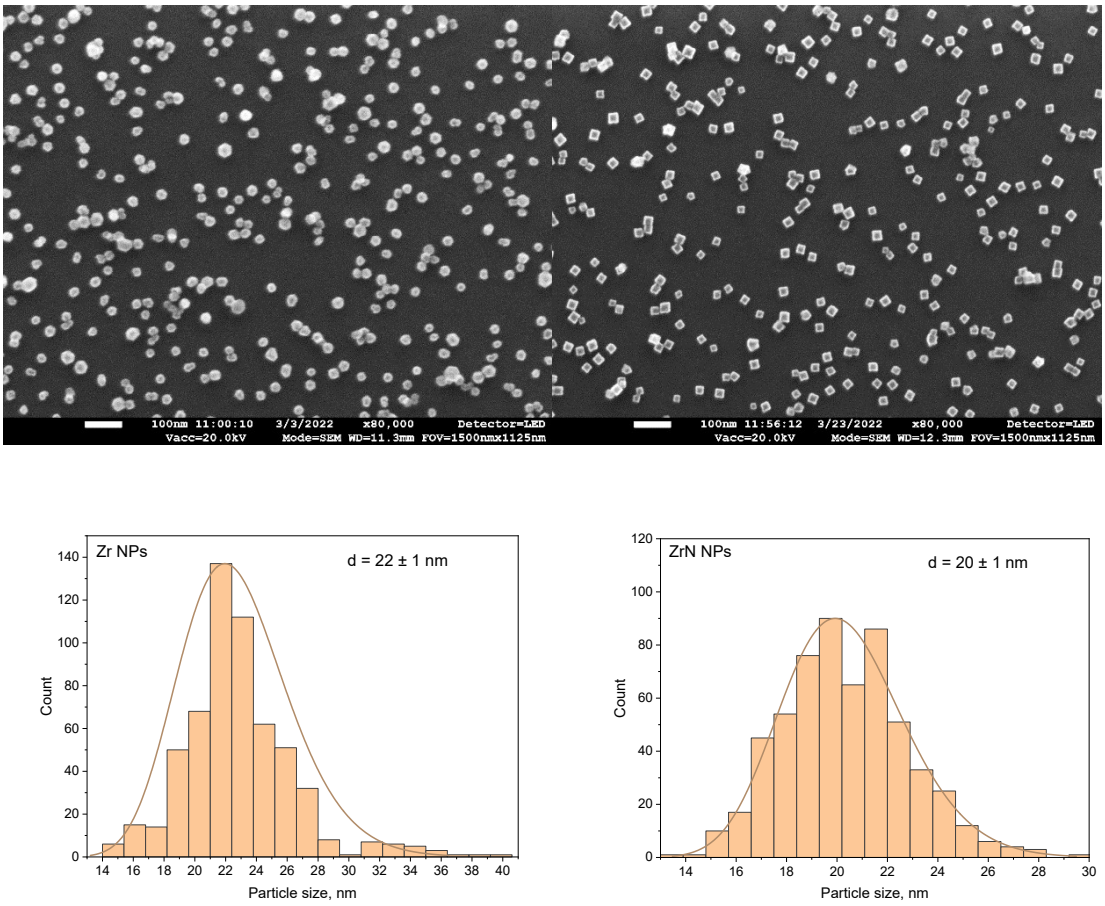

Figure S 2 SEM images and corresponding size histograms of Zr and ZrN NPs deposited on Si. The histograms were fitted by lognormal size distribution functions.

Details of the DFT calculations

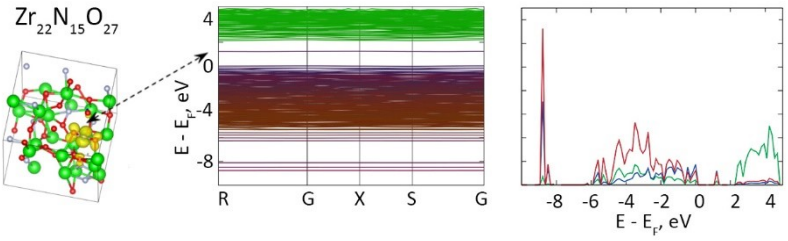

Figure S 3 Formation of the gap state in $Zr_{22}N_{15}O_{27}$ due to N-O hybridization (formation of the Zr-O-N-O-Zr linkage) as obtained by the DFT calculations.

Table S 1 Lattice parameters of ZrN cells (64 atoms in total) with different extent of oxygen substitutions obtained from the DFT calculations.

Sample	Lattice parameters					
	a, Å	b, Å	c, Å	α, deg.	β, deg.	γ, deg.
$Zr_{32}N_{32}$	9.193	9.193	9.193	90.0	90.0	90.0
$Zr_{32}N_{28}O_4$	9.200	9.203	9.200	89.9	89.9	90.1
$Zr_{30}N_{23}O_{11}$	9.180	9.343	9.331	90.0	89.3	90.5
$Zr_{22}N_{15}O_{27}$	9.442	9.447	9.381	90.4	89.1	86.2

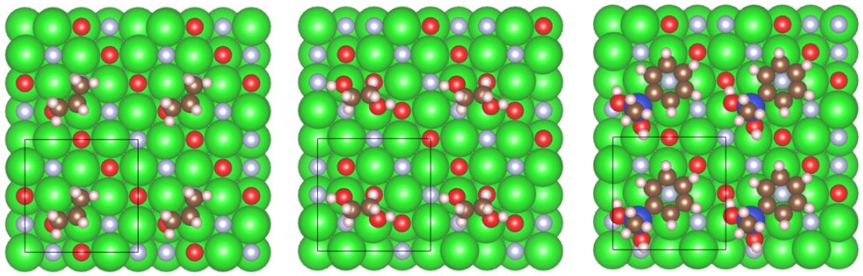

Figure S 4 Relaxed interface geometries of propane, ethylene glycol, and methyl(phenyl)silanediol on the Zr_2NO (100) surface.

Transfer of ZrN NPs from solid supports to liquids by ultrasonication

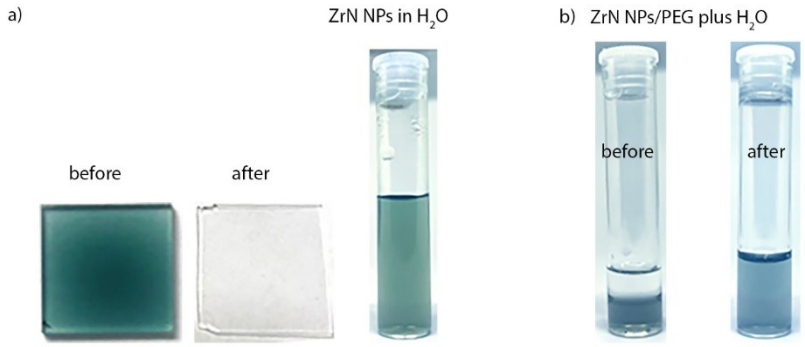

Figure S 5 a) Photos of ZrN NPs deposited on quartz substrate before and after 5-min ultrasonication in distilled H_2O and photo of a vial with the resultant ZrN/H_2O nanofluid; b) photos of the vial with ZrN/PEG nanofluid and H_2O added on top of it before and after 5-min ultrasonication.

UV-Vis measurements of Zr and ZrN NPs deposited on quartz substrates

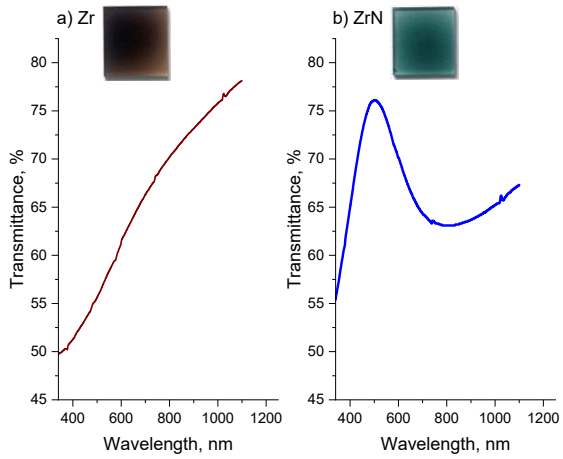

Figure S 6 Optical transmittance spectra of: a) Zr NPs on quartz; b) ZrN NPs on quartz. The insets show the photos of the samples taken against a white background.

Chemical properties of the host liquids

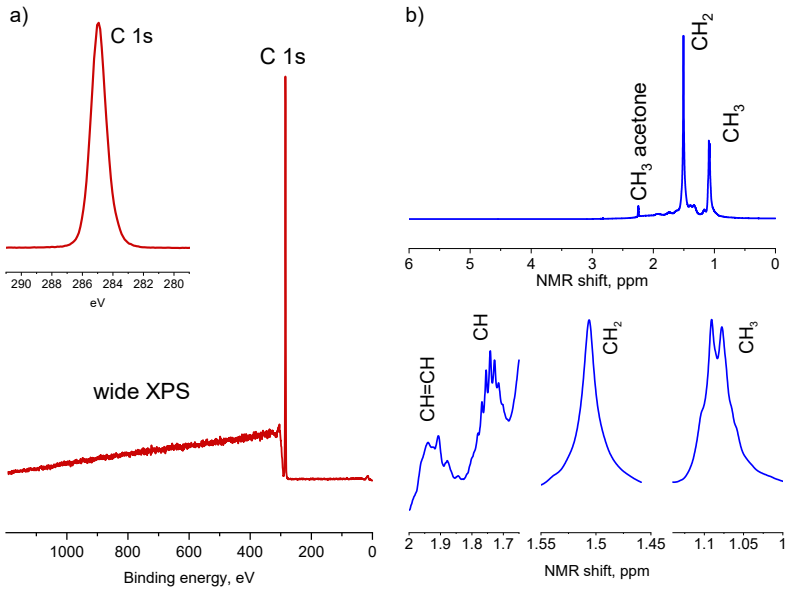

Figure S 7 a) Environmental XPS wide and high-resolution spectra taken directly on liquid paraffin under vacuum of 5×10^{-4} Pa; no other elements except for C are detected; b) NMR ^{1}H wide and selected regions spectra of paraffin in $CDCl_3$.

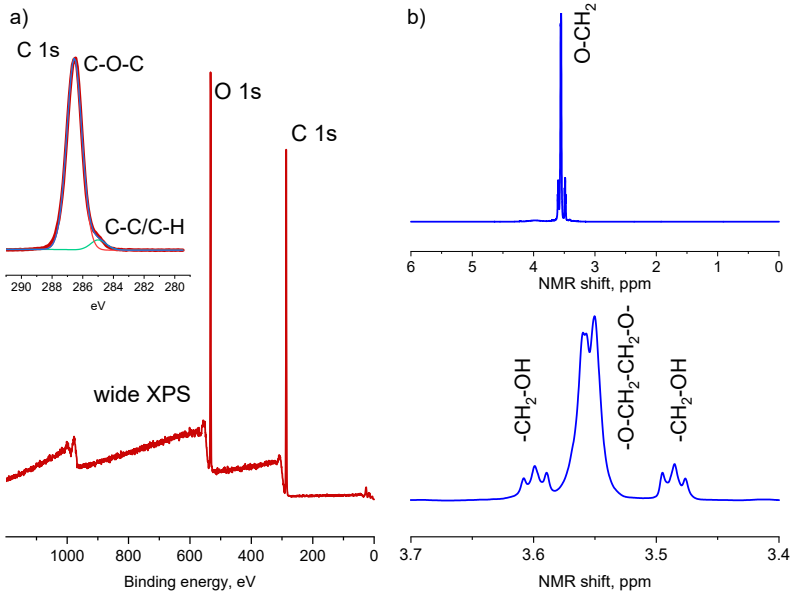

Figure S 8 a) Environmental XPS wide and high-resolution spectra taken directly on liquid PEG under vacuum of 5×10^{-4} Pa; no other elements except for C and O are detected; b) NMR ^{1}H wide and selected regions spectra of PEG in $CDCl_3$. The triplets at 3.6 and 3.5 ppm are associated with the CH_2 units incorporated at the ends of PEG molecule.

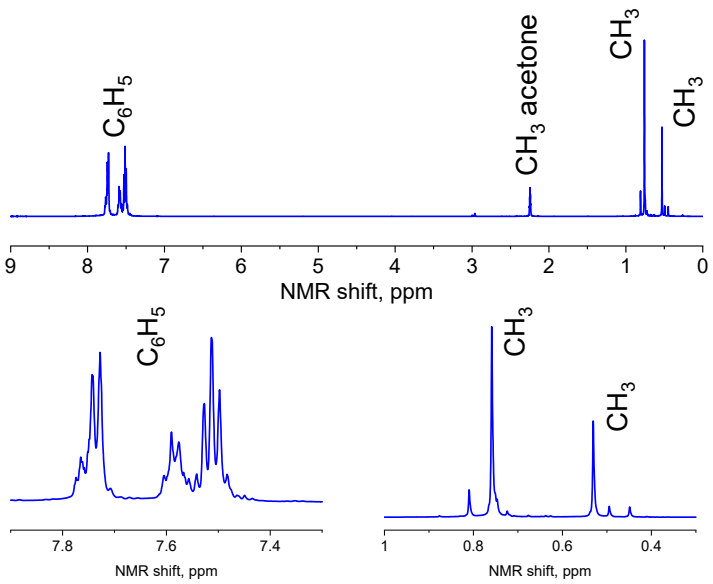

Figure S 9 NMR ^{1}H wide and selected regions spectra of PTT in $CDCl_3$. Small signals at 0.8, 0.5, and 0.45 ppm are related to the CH_3 groups from the impurities in PTT.

Details of the PL measurements and calculations

The PL decay curves at various wavelengths were extracted from the temporally resolved PL measurements. A single exponential decay function was found to fit the data unsatisfactorily; hence, multiexponential functions were chosen to model the PL decays while keeping the number of fitting parameters as low as possible. The PL decay dynamics of the blank solvents was reliably fitted with a two-exponential function, whereas ZrN nanofluids required a three-exponential function. The necessary addition of the third exponential points to the interaction between the NPs and the solvents. The individual decay components of the fits can be found in Table S1 of ESI. Here, the average PL decay times τ_{avg} were extracted from the results of the fits according to Equation S1:

$$\tau_{avg} = \frac{A_1\tau_1^2 + A_2\tau_2^2 + A_3\tau_3^2}{A_1\tau_1 + A_2\tau_2 + A_3\tau_3} \qquad \text{(Equation S1)}$$

Table S 2 PL decay times obtained from fitting of the time-resolved decay curves of ZrN/PEG, Zr/paraffin, and ZrN/PTT nanofluids and the blank solvents.

sample	Excitation	time	Emission	A_1	τ_1, ns	A_2	τ_2, ns	A_3	τ_3, ns	τ_{avg},

	λ, nm	window, ns	λ, nm							ns
PEG	355 nm	100	410 nm	0.958	1.0	0.104	5.1	0.000	0.0	2.46
ZrN/PEG	355 nm	100	410 nm	0.156	15.6	0.890	3.3	0.000	0.0	8.89
ZrN/PEG	355 nm	500	410 nm	1.013	5.8	0.053	39.1	0.000	0.0	14.49
paraffin	355 nm	500	390 nm	0.772	6.1	0.289	56.7	0.000	0.0	45.45
paraffin	325 nm	500	446 nm	0.360	4.7	0.564	18.1	0.081	71.0	34.02
ZrN/paraffin	325 nm	500	443 nm	0.945	4.5	0.005	137.3	0.115	37.8	30.74
ZrN/paraffin	325 nm	500	396 nm	0.900	5.1	0.025	119.8	0.141	29.6	42.97
PPT	325 nm	200	389 nm	0.949	5.0	0.098	14.5	0.000	0.0	7.18
ZrN/PTT	355 nm	500	410 nm	0.188	19.5	0.803	5.9	0.029	155.0	61.22